# Construction of Bifunctional Defect-Engineered UiO-66 Materials and Their Selective Adsorption Mechanism for Anthocyanins

**Xueyu Wang**

***Abstract*— Anthocyanins (ACs), as an important class of natural bioactive compounds, are difficult to separate and purify efficiently due to their structural complexity and subtle differences among homologues[1]. To enhance the molecular recognition ability of adsorbent materials toward anthocyanins, this study introduces 2,5-diaminoterephthalic acid and 2,5-dihydroxyterephthalic acid as organic linkers based on the conventional UiO-66 framework, thereby constructing bifunctionalized materials, namely UiO-66_$(NH_2)_2$ and UiO-66_$(OH)_2$. Subsequently, defect-engineered counterparts, HP-UiO-66_$(NH_2)_2$ and HP-UiO-66_$(OH)_2$ , were obtained via post-synthetic etching[2][3][4].**

**The structures of the as-prepared materials were systematically characterized by X-ray diffraction (XRD), Fourier transform infrared spectroscopy (FT-IR), scanning electron microscopy (SEM), Brunauer–Emmett–Teller (BET) analysis, and thermogravimetric analysis (TGA)[5][6]. Using anthocyanins as model molecules, their adsorption performance and kinetic behavior were further investigated[7][8][9]. The results demonstrate that the synergistic effect of bifunctionalization and defect engineering significantly improves the pore structure and surface chemical environment of the materials, among which HP-UiO-66_$(OH)_2$ exhibits the best adsorption performance[10]. Kinetic studies reveal that the adsorption process follows a pseudo-second-order model and is governed by a multi-stage diffusion mechanism[11][12][13].**

**This work provides a new design strategy for multifunctional MOF-based adsorbents in the separation of natural products.**

## I. Introduction

Anthocyanins are a class of water-soluble natural pigments widely distributed in plants and belong to the flavonoid family[14]. They exhibit various biological activities, including antioxidant, anti-inflammatory, and anticancer effects, and are widely applied in food, pharmaceutical, and functional material fields[15][16]. However, due to their structural diversity and high similarity—particularly the subtle differences in aglycone structures, glycosylation types, and substitution positions—conventional separation methods struggle to achieve efficient and selective purification[17][18][19].

Manuscript received March 26, 2026

**Xueyu Wang**, Dalian Polytechnic University, Dalian, 116034, Liaoning, China

In recent years, metal–organic frameworks (MOFs) have demonstrated great potential in adsorption and separation owing to their high surface area, tunable pore structures, and functionalization capability[20][21]. Among them, UiO-66-based materials have attracted significant attention due to their excellent chemical stability and structural tunability[22]. Previous studies have shown that introducing functional groups such as $–NH_2$ and –OH can effectively regulate the surface polarity and intermolecular interactions of the material, thereby enhancing adsorption performance toward target molecules[23]. However, the regulation ability of single functional groups is limited and often insufficient to meet the requirements for highly selective separation in complex natural product systems[24][25].

Therefore, introducing multiple functional groups to achieve synergistic regulation has emerged as an important strategy for improving material performance[26][27]. Compared with mono-substituted linkers, di-substituted linkers (such as 2,5-diamino and 2,5-dihydroxy terephthalic acids) can provide more active sites, enhancing hydrogen bonding interactions and polarity matching[28][29]. In addition, defect engineering can be employed to construct hierarchical pore structures, which significantly improve the diffusion of large molecules and enhance adsorption efficiency[30][31].

Based on these considerations, this study designed and synthesized UiO-66_$(NH_2)_2$, UiO-66_$(OH)_2$, and their defect-engineered counterparts, HP-UiO-66_$(NH_2)_2$ and HP-UiO-66_$(OH)_2$. Their adsorption behavior and mechanisms toward anthocyanins were systematically investigated[32].

## II. Experimental Section

### 2.1 Chemicals and Materials

Zirconium tetrachloride ($ZrCl_4$), 2,5-diaminoterephthalic acid (BDC-$(NH_2)_2$), 2,5-dihydroxyterephthalic acid (BDC-$(OH)_2$), N,N-dimethylformamide (DMF), formic acid, benzoic acid, methanol, absolute ethanol, and hydrochloric acid were all of analytical grade and used as received without further purification. Anthocyanins (AC) standard compounds were used as the adsorbates. Deionized water was used throughout all experiments.

### 2.2 Instrumentation

The crystal structure of the materials was characterized by powder X-ray diffraction (PXRD). Functional groups were analyzed using Fourier transform infrared spectroscopy (FT-IR). The morphology and microstructure were observed by scanning electron microscopy (SEM) and transmission electron microscopy (TEM), respectively. The specific surface area and pore size distribution were determined by nitrogen adsorption–desorption measurements at 77 K. Thermal stability was evaluated using thermogravimetric

analysis (TGA). The concentration changes of anthocyanins during the adsorption process were further analyzed by high-performance liquid chromatography (HPLC).

2.3 Synthesis of UiO-66_$(NH_2)_2$ and UiO-66_$(OH)_2$

Dual-functionalized UiO-66 materials were synthesized via a solvothermal method. Taking UiO-66_$(NH_2)_2$ as an example, $ZrCl_4$ (150 mg, ~0.64 mmol) was used as the metal source, and 2,5-diaminoterephthalic acid (108 mg, ~0.55 mmol) was used as the organic ligand. Benzoic acid (2.98 g) was added as a modulator, followed by the addition of 10 mL DMF and 50 μL deionized water. The resulting mixture was transferred into a Schott glass bottle and ultrasonicated for 5–10 min to ensure thorough dispersion and dissolution. The mixture was then sealed and heated at 120 °C for 12 h. After the reaction, the system was naturally cooled to room temperature, and the precipitate was collected by centrifugation at 8000 rpm for 8 min.

The obtained solid was first washed with DMF to remove unreacted precursors and residual solvent trapped in the pores. Specifically, the sample was soaked in 10 mL DMF for 8 h, followed by centrifugation, and this process was repeated three times. Subsequently, solvent exchange was performed using methanol, where the sample was soaked in 10 mL methanol for 8 h and centrifuged, repeated three times. Finally, the washed sample was dried in a vacuum oven at 70 °C for 12 h to obtain UiO-66_$(NH_2)_2$.

UiO-66_$(OH)_2$ was synthesized using the same procedure, except that 2,5-dihydroxyterephthalic acid (109 mg, ~0.55 mmol) was used as the ligand. The as-synthesized (non-etched) samples were retained as control adsorbents for subsequent comparison.

2.4 Preparation of HP-UiO-66_$(NH_2)_2$ and HP-UiO-66_$(OH)_2$

To further introduce structural defects and construct hierarchical porosity, the as-synthesized UiO-66_$(NH_2)_2$ and UiO-66_$(OH)_2$ were subjected to post-synthetic etching using formic acid. Specifically, a certain amount of dried UiO-66_$(NH_2)_2$ or UiO-66_$(OH)_2$ was dispersed in 10 mL DMF, followed by the addition of 2.7 mL formic acid. The mixture was ultrasonicated for 5–10 min to ensure uniform dispersion of the sample in the etching system. Subsequently, the reaction mixture was sealed in a Schott glass bottle and heated at 120 °C for 12 h.

After etching, the mixture was naturally cooled to room temperature, and the solid product was collected by centrifugation at 8000 rpm for 8 min. The obtained precipitate was then washed successively with DMF and methanol, with three cycles each. In each washing step, the sample was soaked in 10 mL solvent for 8 h to thoroughly remove residual formic acid, unreacted ligands, and small-molecule byproducts generated during the etching process. Finally, the purified samples were dried in a vacuum oven at 70 °C for 12 h, yielding the defective materials HP-UiO-66_$(NH_2)_2$ and HP-UiO-66_$(OH)_2$.

The purpose of formic acid etching is to partially remove modulator molecules and induce linker or cluster defects within the framework, thereby enhancing pore accessibility and improving mass transfer of large anthocyanin molecules into the internal structure of the MOF.

2.5 Characterization Methods

To elucidate the crystal structure, functional groups, morphology, pore structure, and thermal stability of the four materials, UiO-66_$(NH_2)_2$, UiO-66_$(OH)_2$, HP-UiO-66_$(NH_2)_2$, and HP-UiO-66_$(OH)_2$ were systematically characterized.

Powder X-ray diffraction (PXRD) was employed to analyze the crystalline structure and structural integrity of the materials. The diffraction patterns were typically recorded over a 2θ range of 5°–50° with a scanning rate of 8°·$min^{-1}$, or using standard scanning conditions consistent with previous studies. By comparing the characteristic peak positions and intensities with those of the standard UiO-66 pattern, the effects of dual-functional ligand incorporation and post-etching treatment on framework integrity were evaluated.

Fourier transform infrared spectroscopy (FT-IR) was used to investigate the coordination of carboxylate groups, Zr–O vibrations, and the presence of amino and hydroxyl functional groups. The spectra were recorded in the range of 4000–400 $cm^{-1}$. By comparing the asymmetric and symmetric stretching vibrations of carboxylate groups, Zr–O stretching bands, and the characteristic peaks of –$NH_2$/–OH between pristine and defective samples, the successful incorporation of functional ligands and changes in local coordination environments induced by etching were assessed.

Scanning electron microscopy (SEM) was utilized to observe the surface morphology and particle size of the samples. Prior to measurement, the dried samples were uniformly dispersed and sputter-coated with gold. Images were obtained under appropriate accelerating voltages. By comparing the crystal morphology, particle integrity, and surface roughness of UiO-66_$(NH_2)_2$, UiO-66_$(OH)_2$, and their corresponding HP samples, the influence of defect etching on material morphology was analyzed.

Nitrogen adsorption–desorption measurements were conducted at 77 K to determine the specific surface area, pore volume, and pore size distribution. Before testing, the samples were activated under vacuum to remove guest molecules trapped in the pores. The specific surface area was calculated using the Brunauer–Emmett–Teller (BET) model.

Thermogravimetric analysis (TGA) was performed to evaluate the thermal stability and organic component content of the materials. The measurements were typically carried out under a nitrogen atmosphere from room temperature to 800 °C at a heating rate of 10 °C·$min^{-1}$. By comparing the weight loss behavior of different samples in the medium and high temperature regions, the framework stability and defect degree of pristine and etched materials were analyzed.

2.6 Preparation of Anthocyanin Standard Solutions

A certain amount of anthocyanin standard was accurately weighed and dissolved in deionized water to prepare a stock solution with a defined concentration. The stock solution was stored at 4 °C in the dark for subsequent use. Prior to experiments, the stock solution was diluted stepwise to obtain the desired working solutions.

In this study, an anthocyanin solution with an initial concentration of 120 mg·$L^{-1}$ was used for both static adsorption and kinetic experiments. All solution preparation and adsorption processes were carried out under dark conditions to minimize photodegradation of anthocyanins.

2.7 Static Adsorption Experiments

Batch static adsorption experiments were carried out to evaluate the adsorption performance of the four materials toward anthocyanins. Specifically, 10 mg of adsorbent was accurately weighed and added into a centrifuge tube containing 5 mL of anthocyanin working solution. The adsorption was conducted at room temperature under dark conditions. At predetermined time intervals, samples were withdrawn, centrifuged, and the supernatant was collected to determine the anthocyanin concentration. The sampled solution was then returned to the original system to maintain a constant total volume. The concentration change of anthocyanins over time was used to obtain adsorption kinetic curves and equilibrium adsorption capacities.

The adsorption capacity at time ttt, denoted as $q_t$(mg·g$^{-1}$), was calculated as:

$$q_t = \frac{(C_0 - C_t)V}{m}$$

The equilibrium adsorption capacity $q_e$ (mg·g$^{-1}$) was calculated as:

$$q_e = \frac{(C_0 - C_e)V}{m}$$

where $C_0$,$C_t$ and $C_e$ (mg·L$^{-1}$) represent the initial concentration, concentration at time ttt, and equilibrium concentration of anthocyanins, respectively; V(L) is the volume of the solution; and m (g) is the mass of the adsorbent.

**2.8 Adsorption Kinetics Experiments and Model Fitting**

To compare the adsorption rates and mechanisms of different adsorbents, kinetic experiments were conducted at an initial anthocyanin concentration of 120 mg·L$^{-1}$. According to the experimental results, the adsorption data for all four samples were fitted using pseudo-first-order, pseudo-second-order, and intraparticle diffusion models.

The pseudo-first-order kinetic model is expressed as:

$$ln(q_e - q_t) = lnq_e - k_1 t$$

The pseudo-second-order kinetic model is expressed as:

$$\frac{t}{q_t} = \frac{1}{k_2 q_e^2} + \frac{1}{q_e}$$

The intraparticle diffusion model is given by:

$$q_t = k_i t^{0.5} + C_i$$

Where k1 (min$^{-1}$) is the pseudo-first-order rate constant, k2(g·mg$^{-1}$·min$^{-1}$) is the pseudo-second-order rate constant, and ki(mg·g$^{-1}$·min$^{-1/2}$) is the intraparticle diffusion rate constant. C is a constant related to the thickness of the boundary layer.

By comparing the correlation coefficients ($R^2$) of the fitted models and the agreement between the calculated equilibrium adsorption capacity and the experimental value, the rate-controlling step and the possible adsorption mechanism can be determined.

## III. Results and Discussion

**3.1 Structural Characterization of Materials**

The crystal structures of UiO-66_$(NH_2)_2$, UiO-66_$(OH)_2$ and their corresponding defective materials (HP-UiO-66_$(NH_2)_2$ and HP-UiO-66_$(OH)_2$) were first investigated by PXRD. As shown in Fig. 1, all samples exhibit characteristic diffraction peaks consistent with the typical UiO-66 framework, indicating that the introduction of dual functional groups (–$NH_2$ or –OH) does not destroy the original crystal structure. After formic acid etching, the diffraction peak positions remain unchanged, while the peak intensities slightly decrease, suggesting the successful generation of structural defects without framework collapse.

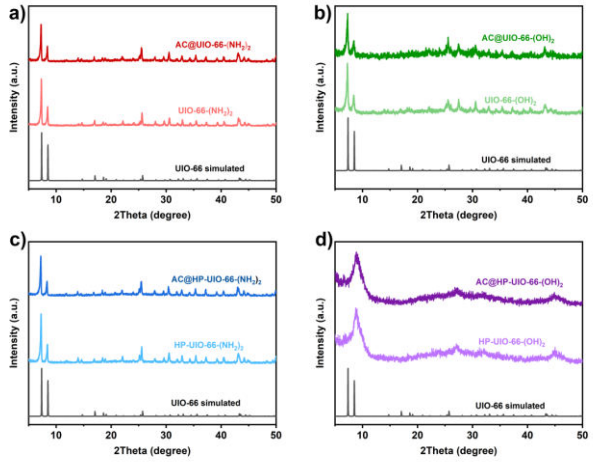


**Figure 1**. (a) PXRD patterns of the synthesized UiO-66_$(NH_2)_2$, AC@UiO-66_$(NH_2)_2$ (b)UiO-66_$(OH)_2$, AC@UiO-66_$(OH)_2$ (c) HP-UiO-66_$(NH_2)_2$, AC@HP-UiO-66_$(NH_2)_2$ (d) HP-UiO-66_$(OH)_2$, AC@HP-UiO-66_$(OH)_2$ compared with the simulated pattern of UiO-66.

FT-IR spectra further confirm the successful incorporation of functional groups. As shown in Fig. 2, the characteristic stretching vibrations of carboxylate groups and Zr–O bonds are clearly observed in all samples. For UiO-66_$(NH_2)_2$, additional absorption bands corresponding to –$NH_2$ groups are detected, while UiO-66_$(OH)_2$ shows enhanced –OH-related signals. After etching, slight shifts in these peaks are observed, indicating changes in the local coordination environment due to defect formation.

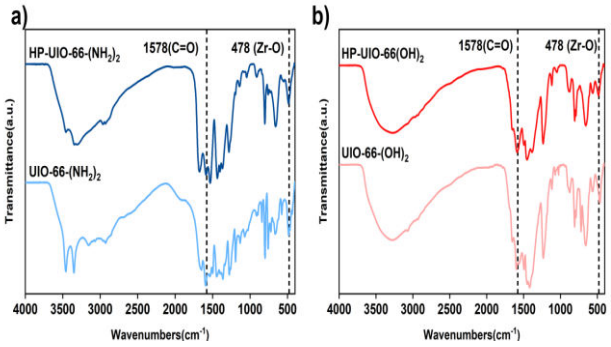


**Figure 2**. FT-IR spectra of (a) UiO-66_$(NH_2)_2$ and HP-UiO-66_$(NH_2)_2$,(b) UiO-66_$(OH)_2$ and HP-UiO-66_$(OH)_2$.

SEM images (Fig. 3) reveal that UiO-66_$(NH_2)_2$ and UiO-66_$(OH)_2$ exhibit well-defined crystalline morphologies with relatively smooth surfaces. In contrast, the etched samples (HP-UiO-66_$(NH_2)_2$ and HP-UiO-66_$(OH)_2$) show rougher surfaces and partially etched textures, indicating the successful formation of defects and increased surface irregularity. This morphological evolution suggests enhanced accessibility of adsorption sites.

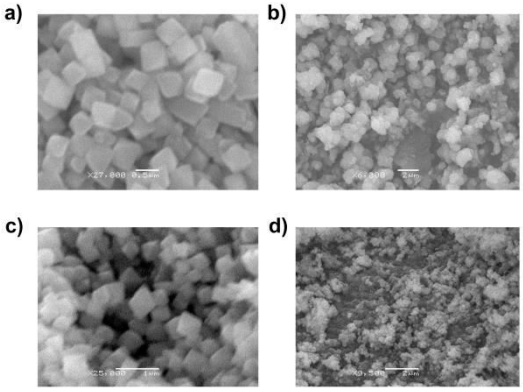


**Figure 3**.SEM images of (a) UiO-66_$(NH_2)_2$,(b)UiO-66_$(OH)_2$,(c) HP-UiO-66_$(NH_2)_2$, (d) HP-UiO-66_$(OH)_2$.

The BET(Fig. 4) analysis results indicate that the specific surface areas of the materials show noticeable differences. Compared with the pristine UiO-66_$(NH_2)_2$ and UiO-66_$(OH)_2$, the formic acid-etched samples, HP-UiO-66_$(NH_2)_2$ and HP-UiO-66_$(OH)_2$, exhibit increased specific surface areas. This suggests that the etching process enhances the accessible surface area of the materials to a certain extent. The introduction of defects is therefore beneficial for exposing more active sites, which in turn facilitates the adsorption process.

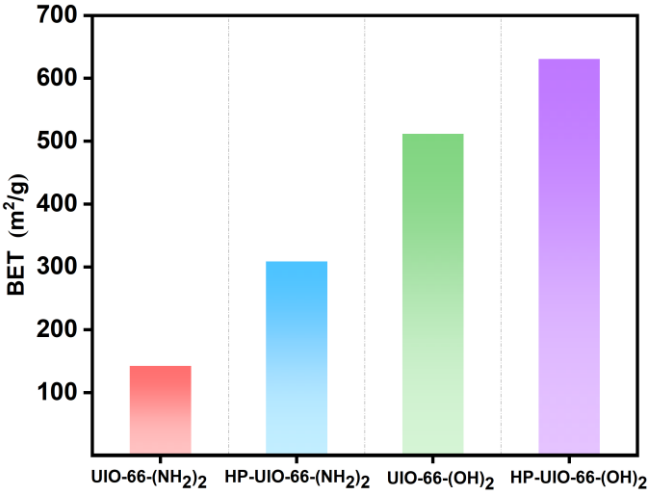


**Figure 4**. Brunauer-Emmett-Teller (BET) surface areas UiO-66_$(NH_2)_2$, UiO-66_$(OH)_2$,HP-UiO-66_$(NH_2)_2$ and HP-UiO-66_$(OH)_2$.

TGA analysis (Fig. 5) shows that all materials maintain good thermal stability, with decomposition occurring at similar temperature ranges. Slight differences in weight loss behavior between pristine and HP samples indicate variations in defect density and organic content.

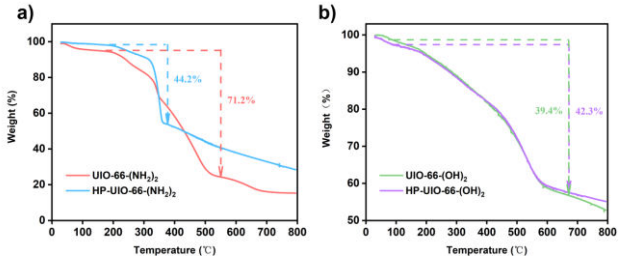


**Figure 5**. TGA curves of (a)UiO-66_$(NH_2)_2$ and HP-UiO-66_$(NH_2)_2$, (b) UiO-66_$(OH)_2$ and HP-UiO-66_$(OH)_2$.

### 3.2 Adsorption Performance toward Anthocyanins

The adsorption performance of the four materials toward anthocyanins was evaluated using HPLC analysis. As shown in Fig. 6, all materials exhibit adsorption capability, but significant differences are observed among them.To further investigate the adsorption behavior and underlying mechanism, the adsorption kinetics of anthocyanins on the four materials were systematically analyzed. The experimental data were fitted using pseudo-first-order, pseudo-second-order, and intraparticle diffusion models, and the corresponding fitting curves are presented in Fig. 7 and Fig. 8. By comparing the fitting results of different kinetic models, the rate-controlling steps and adsorption mechanisms can be better understood.

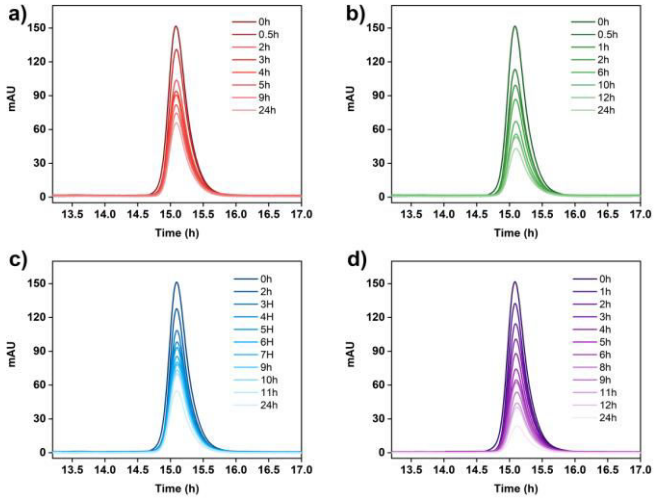


**Figure 6**. HPLC spectra of AC solution (120 mg/L) with different adsorption time for (a)UiO-66_$(NH_2)_2$, (b) UiO-66_$(OH)_2$, (c) HP-UiO-66_$(NH_2)_2$ and (d) HP-UiO-66_$(OH)_2$.

Among the four materials, HP-UiO-66_$(OH)_2$ shows the highest adsorption capacity, followed by HP-UiO-66_$(NH_2)_2$, while the pristine UiO-66 materials exhibit relatively lower adsorption performance. This result clearly demonstrates that both dual functionalization and defect engineering play crucial roles in enhancing adsorption efficiency.

The superior performance of HP-UiO-66_$(OH)_2$ can be attributed to several factors. First, the presence of abundant –OH groups enhances hydrogen bonding interactions with anthocyanin molecules. Second, the increased surface area and hierarchical pore structure facilitate molecular diffusion and improve accessibility to active sites. Third, the enhanced polarity of the material surface improves compatibility with hydrophilic anthocyanins.

In contrast, although $–NH_2$ groups also contribute to hydrogen bonding, their effect is slightly weaker compared to –OH groups in this system. The pristine materials, lacking hierarchical porosity, suffer from diffusion limitations, resulting in lower adsorption capacities.

### 3.3 Synergistic Effect of Dual Functional Groups and Defects

The improved adsorption performance of HP materials can be attributed to the synergistic effect of dual functional

groups and structural defects.The introduction of two functional groups (–$NH_2$ or –OH) increases the number of interaction sites, allowing for stronger and more multiple interactions with anthocyanin molecules. In particular, the –OH groups provide strong hydrogen bonding capability, which is essential for the adsorption of polyphenolic compounds.Meanwhile, defect engineering introduces additional porosity and enhances mass transfer. The formation of mesopores reduces diffusion resistance and allows larger anthocyanin molecules to access internal adsorption sites more easily.

Therefore, the combination of chemical functionality and structural optimization significantly enhances the adsorption performance compared to single-functional or non-defective materials.

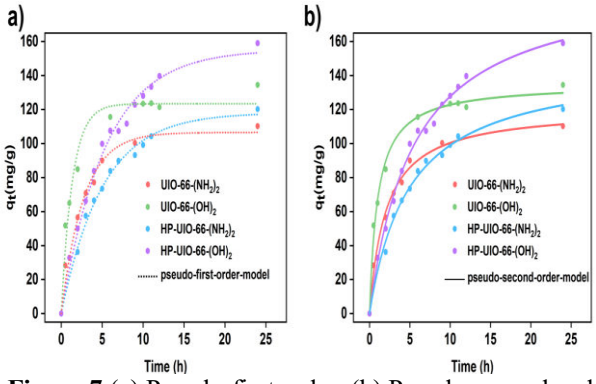


**Figure 7**.(a) Pseudo-first order, (b) Pseudo-second-order fitting of kinetic adsorption isotherms for UiO-66_$(NH_2)_2$, UiO-66_$(OH)_2$, HP-UiO-66_$(NH_2)_2$ and HP-UiO-66_$(OH)_2$.

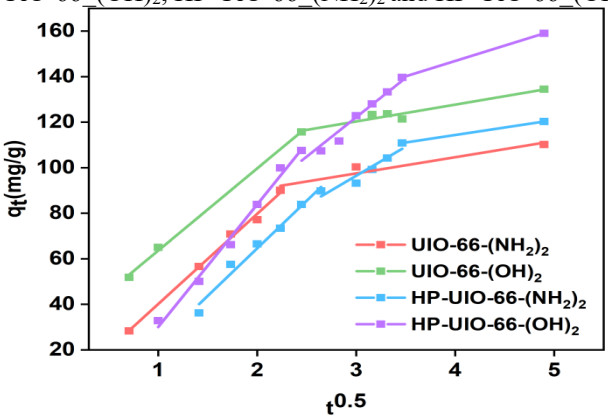


**Figure 8**.Intraparticle diffusion fitting of kinetic adsorption isotherms for UiO-66_$(NH_2)_2$, UiO-66_$(OH)_2$, HP-UiO-66_$(NH_2)_2$ and HP-UiO-66_$(OH)_2$.

;

### 3.4 Adsorption Mechanism

Based on the structural characterization and adsorption results, the adsorption mechanism of anthocyanins on HP-UiO-66 materials can be attributed to the synergistic effect of multiple interactions. Among these, hydrogen bonding plays a dominant role, as the –OH or –$NH_2$ groups on the material surface can form stable hydrogen-bonding networks with the hydroxyl groups of anthocyanin molecules, thereby enhancing adsorption stability. In addition, π–π interactions also contribute significantly to the adsorption process, where the conjugated aromatic structure of anthocyanins can interact with the benzene rings of the MOF ligands through π–π stacking. Furthermore, under certain conditions, anthocyanin molecules carry positive charges while the material surface may exhibit negative charges, leading to electrostatic attraction. The pore structure also contributes through a confinement effect, further promoting the adsorption process. Overall, the adsorption of anthocyanins on HP-UiO-66 materials is governed by the combined effects of hydrogen bonding, π–π interactions, electrostatic attraction, and pore confinement, with hydrogen bonding being the dominant driving force. This also explains the superior adsorption performance of HP-UiO-66_$(OH)_2$.

## IV. Conclusion

In this study, dual-functionalized UiO-66 materials were synthesized using 2,5-diaminoterephthalic acid and 2,5-dihydroxyterephthalic acid as ligands, followed by formic acid etching to obtain defective HP-UiO-66 materials. Their adsorption performance toward anthocyanins was systematically investigated. The results showed that the introduction of dual functional groups did not destroy the crystal structure, while the etching process increased the specific surface area and provided more adsorption sites. The defective materials exhibited significantly enhanced adsorption performance compared to the pristine samples, with HP-UiO-66_$(OH)_2$ showing the best performance. Kinetic analysis indicated that the adsorption followed a pseudo-second-order model, suggesting a chemisorption-controlled process. Mechanistic analysis revealed that hydrogen bonding, π–π interactions, and electrostatic attraction jointly contributed to the adsorption, with hydrogen bonding playing a dominant role. These findings demonstrate that the synergistic effect of dual functionalization and defect engineering effectively enhances the adsorption performance of UiO-66 materials.

## References

[1] Chen Y, et al. Updated Insights into Anthocyanin Stability Behavior from Bases to Cases: Why and Why not Anthocyanins lose during Food Processing. Critical Reviews in Food Science and Nutrition 63, 8639-8671 (2023).

[2] Jiang X, et al. Selective and Controlled Release Responsive Nanoparticles with Adsorption-Pairing Synergy for Anthocyanin Extraction. ACS Nano 18, 2290-2301 (2024).

[3] Yao L, Zhang N, Wang C, Wang C. Highly Selective Separation and Purification of Anthocyanins from Bilberry based on a Macroporous Polymeric Adsorbent. Journal of Agricultural and Food Chemistry 63, 3543-3550 (2015).

[4] Li J, et al. Purification of Propylene and Ethylene by a Robust Metal-Organic Framework Mediated by Host-Guest Interactions. Angewandte Chemie International Edition 60, 15541-15547 (2021).

[5] Na X, Xing S, Tan M, Su W. Fine-Tuning Porous Structure of Zirconium-Based Metal-Organic Frameworks for Efficient Separation and Purification of Astaxanthin by Defect Engineering. Advanced Science (Weinh) 11, e2409451 (2024).

[6] Smith GL, et al. Reversible Coordinative Binding and Separation of Sulfur Dioxide in a Robust Metal-Organic Framework with Open Copper Sites. Nature Materials 18, 1358-1365 (2019).

[7] Frisch M, Trucks G, Schlegel H, Scuseria G, Robb M, Cheeseman J, Scalmani G, Barone V, Mennucci B, Petersson G, Gaussian 09, 9, 227 (2009).

[8] Torimoto A, Ishibashi D, Yamashita A, Uemura T, Hosono N. High-Precision Separation and Refinement of Fatty Acid Derivatives by Metal-Organic Frameworks. Journal of the American Chemical Society 147, 17228-17238 (2025).

[9] Wen Y, Chen H, Zhou X, Deng Q, Zhao C, Gong X. A Polyamide Resin based Method for Adsorption of Anthocyanins from Blackberries. New Journal of Chemistry 40, 3773-3780 (2016).
[10] Liu Y, Zhang Y, Zhou Y, Feng X-s. Anthocyanins in Different Food Matrices: Recent Updates on Extraction, Purification and Analysis Techniques. Critical Reviews in Analytical Chemistry 54, 1430-1461 (2022).
[11] Koh J, Xu Z, Wicker L. Binding Kinetics of Blueberry Pectin-Anthocyanins and Stabilization by Non-Covalent Interactions. Food Hydrocolloids 99, 105354 (2020).
[12] Sandhu AK, Gu L. Adsorption/Desorption Characteristics and Separation of Anthocyanins from Muscadine (Vitis rotundifolia) Juice Pomace by Use of Macroporous Adsorbent Resins. Journal of Agricultural and Food Chemistry 61, 1441-1448 (2013).
[13] Li B, et al. An Ideal Molecular Sieve for Acetylene Removal from Ethylene with Record Selectivity and Productivity. Advanced materials 29, 1704210 (2017).
[14] More PR, Jambrak AR, Arya SS. Green, Environment-Friendly and Sustainable Techniques for Extraction of Food Bioactive Compounds and Waste Valorization. Trends in Food Science & Technology 128, 296-315 (2022).
[15] Li S, Han W, An QF, Yong KT, Yin MJ. Defect Engineering of MOF-Based Membrane for Gas Separation. Advanced Functional Materials 33, 2303447 (2023).
[16] Wang Y, et al. One-step Ethylene Purification from an Acetylene/Ethylene/Ethane Ternary Mixture by Cyclopentadiene Cobalt-Functionalized Metal-Organic Frameworks. Angewandte Chemie International Edition 60, 11350-11358 (2021).
[17] Sun H, Jin Z, Yang C, Akkermans R. L. C, Robertson S. H, Spenley N. A, Miller S, Todd S. M, "COMPASS II: extended coverage for polymer and drug-like molecule databases", Journal of Molecular Modeling, 22, 1-10 (2016).
[18] Corella-Ochoa MN, et al. Homochiral Metal-Organic Frameworks for Enantioselective Separations in Liquid Chromatography. Journal of the American Chemical Society 141, 14306-14316 (2019).
[19] Tosi, M. P., Evaluation of electrostatic lattice potentials by the Ewald method, Solid State Physics, 16, 107 (1964).
[20] Lu T, Multiwfn: A multifunctional wavefunction analyzer, The Journal of Computational Chemistry 33, 580-592 (2012).
[21] Dangles O. Anthocyanins as Natural Food Colorings: The Chemistry Behind and Challenges Still Ahead. Journal of Agricultural and Food Chemistry 72, 12356-12372 (2024).
[22] Du W, et al. An Anionic Sod-type Terbium-MOF with Extra-Large Cavities for Effective Anthocyanin Extraction and Methyl Viologen Detection. Chemical Communications (Camb) 54, 5972-5975 (2018).
[23] Zhou HC, Kitagawa S. Metal-organic frameworks (MOFs). Chemical Society Reviews 43, 5415-5418 (2014).
[24] Bueno JM, Sáez-Plaza P, Ramos-Escudero F, Jiménez AM, Fett R, Asuero AG. Analysis and Antioxidant Capacity of Anthocyanin Pigments. Part II: Chemical Structure, Color, and Intake of Anthocyanins. Critical Reviews in Analytical Chemistry 42, 126-151 (2012).
[25] Foroutani Z, Afshar Mogaddam MR, Ghasempour Z, Ghareaghajlou N. Application of Deep Eutectic Solvents in the Extraction of Anthocyanins: Stability, Bioavailability, and Antioxidant property. Trends in Food Science & Technology 144, 104324 (2024).
[26] Li R, et al. Systematic Study on the Removal of Per- and Polyfluoroalkyl Substances from Contaminated Groundwater Using Metal-Organic Frameworks. Environmental science & technology 55, 15162-15171 (2021).
[27] Freund R, et al. The Current Status of MOF and COF Applications. Angewandte Chemie International Edition 60, 23975-24001 (2021).
[28] Nosé, S. A unified formulation of the constant temperature molecular dynamics methods, The Journal of Chemical Physics, 81, 511-519 (1984)
[29] Tan C, Dadmohammadi Y, Lee MC, Abbaspourrad A. Combination of Copigmentation and Encapsulation Strategies for the Synergistic Stabilization of Anthocyanins. Comprehensive Reviews in Food Science and Food Safety 20, 3164-3191 (2021).
[30] Castañeda-Ovando A, Pacheco-Hernández MdL, Páez-Hernández ME, Rodríguez JA, Galán-Vidal CA. Chemical studies of anthocyanins: A review. Food Chemistry 113, 859-871 (2009).
[31] Wang H, et al. Topologically Guided Tuning of Zr-MOF Pore Structures for Highly Selective Separation of C6 Alkane Isomers. Nature Communications 9, 1745 (2018).
[32] Zang Z, et al. An Updated Review on the Stability of Anthocyanins Regarding the Interaction with Food Proteins and Polysaccharides. Comprehensive Reviews in Food Science and Food Safety 21, 4378-4401 (2022).